

A CaO₂@Tannic Acid-Fe^{III} Nanoconjugate for Enhanced Chemodynamic Tumor Therapy

Fei Chen,^[a] Beibei Yang,^[a] Lan Xu,^[a] Jinfeng Yang,^{*,[b]} and Jishan Li^{*,[a]}

Chemodynamic therapy (CDT) is an effective tumor treatment strategy in which Fe^{II} reacts with hydrogen peroxide (H₂O₂) in tumor cells to produce highly toxic hydroxyl radical ([•]OH) through the Fenton reaction. However, the content of endogenous H₂O₂ in cells is limited, and the reaction between Fe^{III} and H₂O₂ is inefficient, greatly limiting the efficiency of the Fenton reaction and reducing the effectiveness of tumor treatment. Therefore, in this work, we designed and synthesized a new type of nano-system (CaO₂@TA-Fe^{III}) for the enhanced CDT of tumors, in which the polyphenolic compound- tannic acid (TA) and Fe^{III} formed a TA-Fe nano-coating on the surface of calcium peroxide (CaO₂) nanospherical aggregates. When the CaO₂@TA-Fe^{III} nanoconjugates reach the tumor site, the CaO₂ contained in

the nanoconjugates produces H₂O₂ after disintegration in tumor cells, and the carried TA rapidly reduces Fe^{III} to Fe^{II}, solving the two major shortcomings in CDT of (1) insufficient content of H₂O₂ in cancer cells, and (2) low catalytic efficiency of the Fenton reaction. Additionally, the [•]OH produced in the Fenton reaction induces oxidative stress for the tumor cells, promoting the occurrence of the “calcium overload” process, and thereby accelerating the death of tumor cells. Experimental results in vitro and in vivo showed that CaO₂@TA-Fe^{III} nanoconjugates can effectively kill cancer cells and display an excellent tumor therapeutic effect. We believe that the CaO₂@TA-Fe^{III} nanoconjugates are a promising new nano-platform for highly effective tumor treatment.

Introduction

Many metal ions play a highly important role in biological activities and participate in cell proliferation and metabolism. When the content of these metal ions in the living organism is unbalanced, it will affect the normal biological activities of the cells and even induce cell death.^[1–2] Iron ion is a typical example of this phenomenon. Iron is an essential trace element in the body and plays an extremely important role in maintaining the body's health. On the one hand, iron-deficiency anaemia is still a serious threat to global human health; on the other hand, a too high content of iron ions can promote the formation of free radicals that can cause cell death.^[3–8]

In recent years, many researchers have proposed various nano-systems using iron-dependent accumulation of hydroxyl radicals ([•]OH) to perform Chemodynamic therapy (CDT).^[9–12] Excessive iron ions will react with hydrogen peroxide (H₂O₂) overexpressed in cancer cells and induce the formation of hydroxyl radicals ([•]OH) through the Fenton reaction. Among the various forms of reactive oxygen species (ROS), [•]OH gives rise to the strongest damage of biological systems.^[13] In the cell,

[•]OH can in situ attack and oxidize biological macromolecules including unsaturated fatty acids, amino acids and DNA, thereby enabling CDT treatment of cancer cells.^[14–18] Compared to cancer treatment strategies such as photodynamic therapy (PDT) and photothermal therapy (PTT) that have emerged in the past few decades, CDT neither requires a light source nor is affected by the local oxygen content.^[19–22] However, both the limited intracellular H₂O₂ content and the inefficient catalysts limit the efficiency and further applications of CDT in cancer treatment. Therefore, there is still a great need to develop Fenton nano- systems with excellent performance for effective cancer treatment.

In addition to the iron-mediated Fenton reaction-based CDT, recent studies have reported the potential application of other metal ions to tumor therapy, for example Mn^{II}, Cu^{II}, and Co^{II}.^[23–27] These metal ions can perform Fenton-like reactions with H₂O₂ overexpressed in tumor cells, and can produce ROS, thereby carrying out tumor treatment. This has also inspired researchers to further study other functional metal ions and develop new effective cancer treatment strategies. Recently, Bu's group designed pH-sensitive calcium peroxide (CaO₂) nanoparticles and used them for cancer treatment. Their research showed that a rapid release of calcium ions in a weak acidic tumor environment can effectively induce “calcium overload”, carrying out ion interference therapy on tumor cells.^[28] This study revealed the possibility of the use of other metal ions in tumor treatment and pointed out a new direction for cancer treatment.

Tannic acids (TA) are natural polyphenols derived from plants that are approved by the United States Food and Drug Administration (FDA) and are widely used in food and medicine.^[29] As a common polyphenol, TA shows good adhesion to solid materials, and can rapidly form a metal

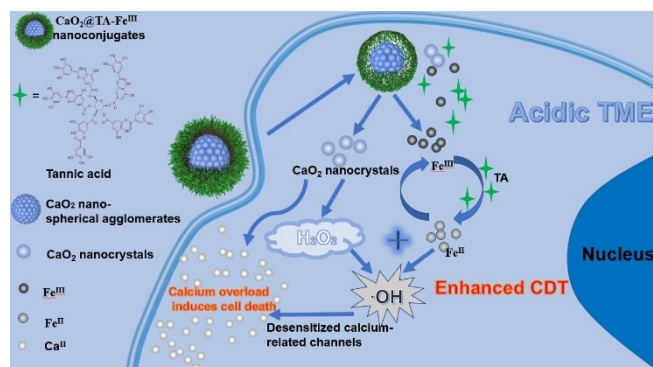
[a] F. Chen, B. Yang, L. Xu, Prof. J. Li
State Key Laboratory of Chemo/Biosensing and Chemometrics
College of Chemistry and Chemical Engineering
Hunan University
Changsha 410082 (China)
E-mail: jishanli@hnu.edu.cn

[b] Prof. J. Yang
Tumor Hospital
Xiangya School of Medicine
Central South University
Changsha 410013 (China)
E-mail: 346405681@qq.com

 Supporting information for this article is available on the WWW under <https://doi.org/10.1002/cmdc.202100108>

polyphenol network structure through coordination with metal ions in aqueous solution.^[30–31] In the presence of an interface of solid materials, TA and metal ions can adhere to the interface to form a capsule nano-coating.^[32–33] In addition, many studies have confirmed that the coordination between metal ions and phenolic hydroxyl groups of polyphenols is pH-dependent.^[34] The network structure formed by TA and Fe³⁺ is a typical example. For pH < 2, TA and Fe^{III} mainly exist as mono-complex, for 3 < pH < 6, TA and Fe^{III} mainly exist as bis-complex, and for pH > 7, TA and Fe^{III} mainly exist as tris-complex.^[35] Therefore, the stability of capsule-like coatings obtained by self-assembly of metal ions and polyphenols is also pH-dependent.^[36–37] This characteristic has received widespread attention in the field of drug delivery.^[38–40]

Based on the above background, we designed a novel nanoconjugate of CaO₂@TA-Fe^{III} that can be synthesized easily and rapidly, and applied it for the enhanced CDT of tumors (Scheme 1). We first synthesized CaO₂ nano-spherical agglomerates, and then used Fe^{III} and TA to form a dense TA-Fe nanocoating on the surface of the CaO₂ nanosphere agglomerates. When the CaO₂@TA-Fe^{III} nanoconjugates entered the tumor cells, the TA-Fe nano coating disintegrated in the weak acidic microenvironment of the tumor, the internal CaO₂ nanosphere agglomerates are exposed and hydrolysed to produce H₂O₂, and TA reduced Fe^{III} to Fe^{II} rapidly, solving the problem of limited Fenton reaction due to the limited content of endogenous H₂O₂ and low efficiency of the Fenton reaction catalyst. At the same time, the [•]OH produced by the reaction between Fe^{III} and H²O₂ gives rise to an oxidative stress state of the tumor cells that desensitized the cell's calcium ion protein, leading to the process of calcium overload and accelerating the death of the cancer cells.^[28,41–42] The [•]OH generated during the Fenton reaction mediated by Fe^{III} and the "Ca^{II} overload" interact synergistically with each other, greatly improving the tumor cytotoxicity.



Scheme 1. Schematic illustration of CaO₂@TA-Fe^{III} nanoconjugates for enhanced CDT of tumor.

Results and Discussion

Synthesis and characterization of the CaO₂@TA-Fe^{III} nanoconjugates

The CaO₂ nanosphere agglomerates were synthesized by one-pot method according to the previous report in the literature.^[43] As shown in Figure 1A, the synthesized CaO₂ nanosphere agglomerates were spherical and uniform with a size of approximately 90 nm. Then, TA and Fe^{III} were used to form a TA-Fe nano-coating on the surface of the CaO₂ nanospheres. As shown in Figure 1B, the morphology of the CaO₂@TA-Fe^{III} nanoconjugates was still a relatively uniform spherical shape with a size of approximately 100 nm. Dynamic light scattering (DLS) measurements (Figure 1C) indicated that the size distribution of the CaO₂ nanosphere agglomerates was narrow with an average hydrodynamic diameter of 94 nm, while the CaO₂@TA-Fe^{III} nanoconjugates has an average hydrodynamic diameter of 188 nm. Moreover, it is observed from Figure 1D that the zeta potential of CaO₂ nanospheres was 4.66 mV, while the zeta potential of CaO₂@TA-Fe^{III} nanoconjugates was −14.60 mV. The change of both the average hydrodynamic diameter and zeta potential of the nanoparticles indirectly indicated that the surface of CaO₂ nanospheres was successfully coated with the

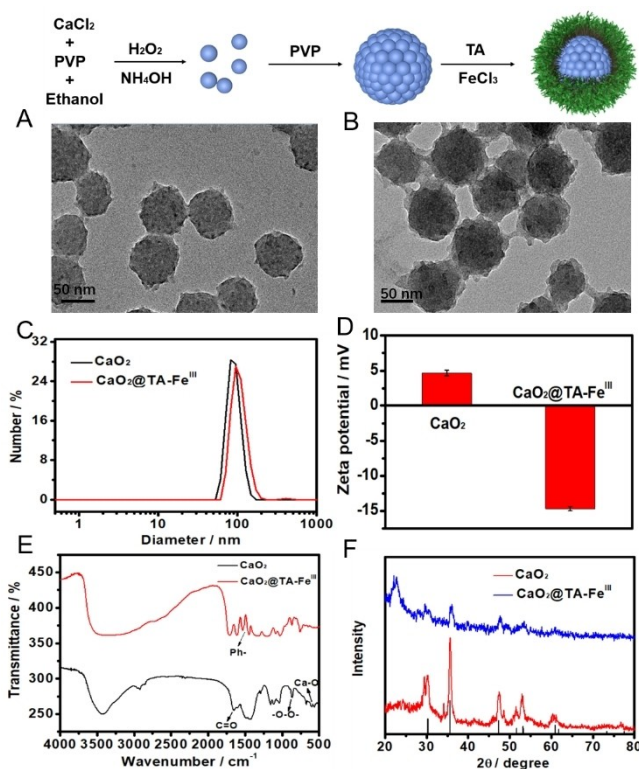


Figure 1. Synthesis process of CaO₂@TA-Fe^{III} nanoconjugates. (A) TEM image of the CaO₂ nanosphere agglomerates and (B) the CaO₂@TA-Fe^{III} nanoconjugate. (C) Hydrodynamic size distribution and (D) zeta potential of the CaO₂ nano spherical agglomerates and the CaO₂@TA-Fe^{III} nanoconjugates. (E) FT-IR spectrum of the as-synthesized CaO₂ nanosphere agglomerates and the CaO₂@TA-Fe^{III} nanoconjugates. (F) X-ray powder diffraction pattern of the CaO₂ nanosphere agglomerates and the CaO₂@TA-Fe^{III} nanoconjugates. The data are represented as mean ± S.D. of three independent experiments

TA-Fe nanocoating. In addition, the Fourier transform infrared (FTIR) absorption spectrum of the CaO_2 nanosphere agglomerates showed that the absorption peak at 570 cm^{-1} was due to the O–Ca–O vibration,^[43–44] and the absorption peak at approximately 1646 cm^{-1} was derived from the stretching of the C=O bond, indicating the presence of PVP on the CaO_2 surface (Figure 1E). The infrared absorption peak of $\text{CaO}_2@TA\text{-Fe}^{\text{III}}$ nanoconjugates at $1400\text{--}1600\text{ cm}^{-1}$ was due to the existence of benzene ring, and provided additional indirect proof for the presence of a TA-Fe nanocoating on the surface of CaO_2 . The powder X-ray diffraction (XRD) pattern showed that the diffraction peaks of the synthesized CaO_2 nanosphere aggregates were consistent with the tetragonal CaO_2 standard card (PDF#03-0865) (Figure 1F), showing that the CaO_2 nanospheres were obtained successfully. In addition, an examination of the diffraction pattern of the $\text{CaO}_2@TA\text{-Fe}^{\text{III}}$ nanoconjugates showed that the diffraction peak of the CaO_2 crystal was still retained, indicating that the formation of the TA-Fe nanocoating did not change the crystal structure of CaO_2 nanospheres.

pH-dependent decomposition of CaO_2 nanospheres

The decomposition of CaO_2 spherical nanoaggregates into H_2O_2 in phosphate buffer solutions with different pH values (pH 7.4, 6.0, 5.0) was detected by the titanium sulphate colorimetric method.^[45] Within 48 h, only 33.01% of the CaO_2 nanospheres was decomposed to produce H_2O_2 at pH 7.4, whereas a higher amount of CaO_2 nanospheres was decomposed into H_2O_2 in the weak acidic microenvironment, with 57.97% and 87.235% decomposition obtained at pH 6.0 and 5.0, respectively (Figure 2A). The experimental results showed that the synthesized CaO_2 nano-sphere aggregates had a good pH response that was consistent with the previous reports about CaO_2 .^[28,43,46] According to the literature, the CaO_2 nanosphere aggregates are formed by the agglomeration of many CaO_2 nanocrystals due to the better stability of the aggregates compared to single CaO_2 nanocrystals, thus making the aggregates more suitable for use in biomedical applications.^[43] Therefore, we chose the CaO_2 nano-sphere aggregates as the H_2O_2 source.

TA-triggered generation of Fe^{II} from the $\text{CaO}_2@TA\text{-Fe}^{\text{III}}$ nanoconjugates

For the $\text{CaO}_2@TA\text{-Fe}^{\text{III}}$ nanoconjugates, TA acts as a reducing agent, and should accelerate the conversion of Fe^{III} to Fe^{II} . Therefore, the reducing capacity of TA was verified. First, the generation of Fe^{II} was measured using the classic 1,10-phenanthrene method. As shown in Figure 2B, in the presence of TA, 47.90% of Fe^{III} was reduced to Fe^{II} within 3 h, while almost no Fe^{II} was detected in the absence of TA. The above results show that TA can efficiently realize the conversion of Fe^{III} to Fe^{II} . Then, the generation of Fe^{II} from the $\text{CaO}_2@TA\text{-Fe}^{\text{III}}$ nanoconjugates over time was examined. Within 3 h, 56.30% of Fe^{II} was detected, and the release of Fe^{II} was time-dependent (Figure 2C). As a control, we mixed the CaO_2 nanospheres

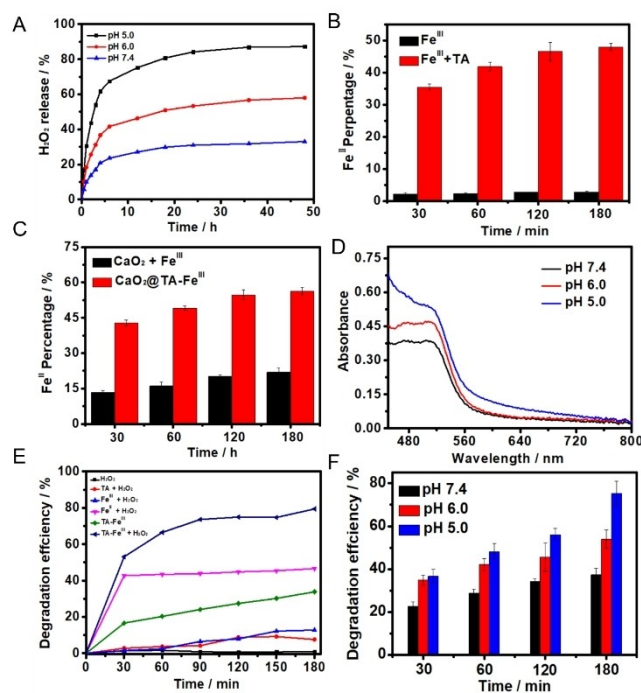


Figure 2. (A) Time-dependent H_2O_2 release from the CaO_2 nanosphere agglomerates dispersed in buffer solutions with different pH (the standard curve is shown in Figure S1); (B–C) Time-dependent generation of Fe^{II} from the Fe^{III} , $\text{Fe}^{\text{III}} + \text{TA}$, $\text{CaO}_2 + \text{Fe}^{\text{III}}$, and $\text{CaO}_2@TA\text{-Fe}^{\text{III}}$ (the standard curve is shown in Figure S2); (D) UV-vis spectra of the solution containing 1,10-phenanthroline and $\text{CaO}_2@TA\text{-Fe}^{\text{III}}$ in buffer solutions with different pH; (E) Detection of $\cdot\text{OH}$ using MB in the presence of different species (TA, Fe^{III} , Fe^{II} , $\text{TA}\text{-Fe}^{\text{III}}$) upon addition of H_2O_2 ; (F) Degradation rate of MB by the $\text{CaO}_2@TA\text{-Fe}^{\text{III}}$ under different pH. The data are represented as mean \pm S.D. of three independent experiments.

solution with Fe^{III} , but only a small amount of Fe^{II} was detected. In addition, the generation of Fe^{II} from $\text{CaO}_2@TA\text{-Fe}^{\text{III}}$ nanoconjugates in phosphate buffer solutions with different pH values (pH 7.4, 6.0, 5.0) was also examined. As shown in Figure 2D, more Fe^{II} is released under weak acid condition, possibly due to the degradation of the $\text{CaO}_2@TA\text{-Fe}^{\text{III}}$ nanoconjugates under weak acid conditions that leads to the release of TA and Fe^{III} and the subsequent electron transfer process between TA and Fe^{III} that results in the conversion of Fe^{III} to Fe^{II} .^[41,47]

Fenton reaction with the $\text{CaO}_2@TA\text{-Fe}^{\text{III}}$ nanoconjugates

The improved Fenton reaction ability of TA-Fe system was verified by methylene blue (MB) colorimetric method.^[47] As shown in Figure 2E, in the presence of H_2O_2 , the degradation rate of MB by the TA-Fe complex, Fe^{II} , Fe^{III} , and TA in 180 min were 79.07%, 46.13%, 12.82%, and 7.62%, respectively, while as a control, obvious degradation of MB was not observed when only H_2O_2 was presented, demonstrating the significant Fenton reaction enhanced performance of the TA-Fe system. Then, the ability of TA-Fe complex to catalyze H_2O_2 to produce $\cdot\text{OH}$ in different pH conditions was also investigated. As shown

in Figure S3, within 180 min, the MB degradation efficiency by the TA-Fe complex in PBS solution with pH of 7.4, 6.0 and 5.0 was 25.03 %, 50.16%, and 68.18%, respectively, further indicating that the TA-Fe complex system has the ability to catalyze H_2O_2 to produce *OH efficiently, and moreover, the efficiency of TA-Fe complex to catalyze H_2O_2 is pH-dependent, because TA can reduce Fe^{III} to Fe^{II} quickly under the condition of weak acid,^[40,47] thus greatly improving the reaction efficiency of Fenton reaction. Next, the Fenton reaction ability of the $CaO_2@TA-Fe^{III}$ nanoconjugates in vitro was examined by MB degradation experiment. As shown in Figure 2F, the degradation efficiency of MB by $CaO_2@TA-Fe^{III}$ nanoconjugates in PBS buffer solution was only 37.32% at pH 7.4 within 180 min, while the catalytic capacity was relatively strong in the weak acidic environment, with the degradation rate of 53.04% at pH 6.0 and 75.33% at pH 5.0, respectively. All the together experimental results showed that the Fenton effect of the $CaO_2@TA-Fe^{III}$ nanoconjugates was pH-responsive, which was consistent with our expected results.

Cellular uptake of $CaO_2@TA-Fe^{III}$ nanoconjugates

Next, the uptake ability of $CaO_2@TA-Fe^{III}$ nanoconjugates by using 4T1 cells as a model was investigated. First, the cells were incubated with $CaO_2@TA-Fe^{III}$ nanoconjugates labeled with fluorescein isothiocyanate (FITC) for 2, 4, and 8 h, respectively. Then, the intensity of green fluorescence in the 4T1 cells was detected by confocal microscope. The stronger the fluorescence emission, the greater the amount of $CaO_2@TA-Fe^{III}$ nanoconjugates taken up by the cells. One can conclude from Figure 3

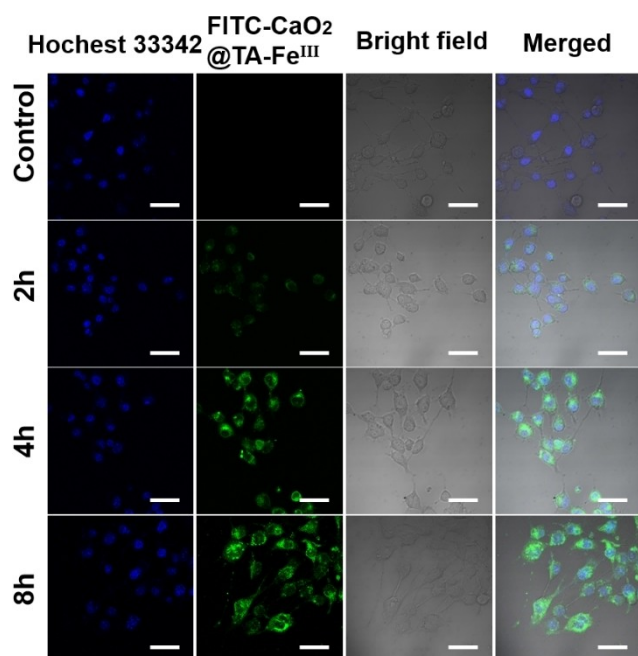


Figure 3. CLSM images of 4T1 cells after co-incubation with FITC- $CaO_2@TA-Fe^{III}$ nanoconjugates for 2, 4, 8 hours. (green fluorescence: FITC- $CaO_2@TA-Fe^{III}$ nanoconjugates, blue fluorescence: Hoechst 33342. Scar bar: 20 μm).

that as the incubation time increased, the amount of $CaO_2@TA-Fe^{III}$ nanoconjugates taken up by the cells increased. When the cells were incubated with the FITC-labeled $CaO_2@TA-Fe^{III}$ nanoconjugates for 2 h, weak green fluorescence began to appear. The group incubated for 4 h showed strong green fluorescence emission. At the same time, we can also see that the green fluorescence intensity of the group incubated for 8 h was not much different from the group incubated for 4 h. This showed that the endocytosis of $CaO_2@TA-Fe^{III}$ nanoconjugates was saturated by 4T1 cells after 4 h. Therefore, we incubated the cells for 4 h in the next cell experiments. The above experimental results also proved that 4T1 cells can take in $CaO_2@TA-Fe^{III}$ nanoconjugates efficiently, which was also the basis for $CaO_2@TA-Fe^{III}$ nanoconjugates to kill cancer cells efficiently.

Demonstration of ROS generation and calcium overload of $CaO_2@TA-Fe^{III}$ nanoconjugates

The ROS generation ability of the $CaO_2@TA-Fe^{III}$ nanoconjugates in cells (using the 4T1 cell as the model) was first investigated using the DCFH-DA ROS detection kit. As shown in Figure 4A, compared to the control group, only very slight fluorescence emission can be observed for the cells treated with the TA-Fe complex (30 $\mu g/mL$), and then the fluorescence emission

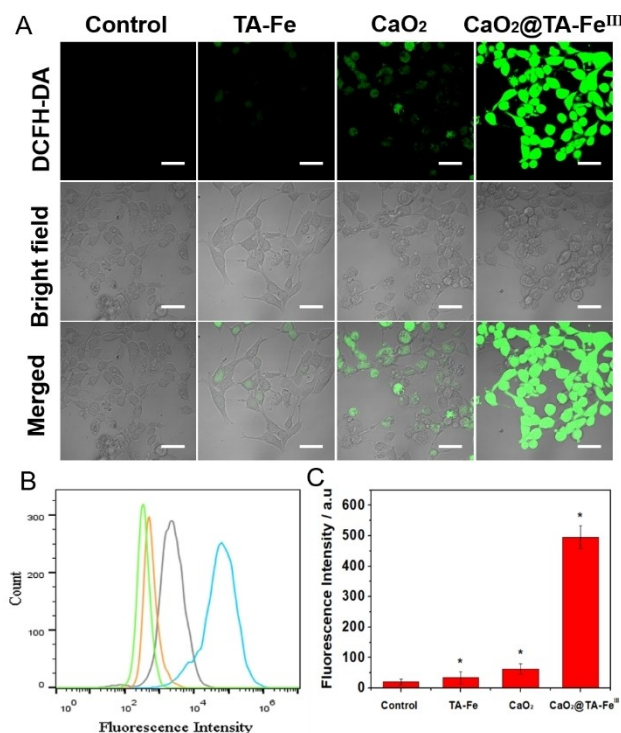


Figure 4. (A) Fluorescence imaging and (B) flow cytometry of 4T1 cells treated with DCFH-DA and the TA-Fe complex, CaO_2 nanoparticles, and $CaO_2@TA-Fe^{III}$ nanoconjugates, respectively. (C) Quantitative analysis of the fluorescence intensity was resulted from 'B' ($\lambda_{ex/em} = 488/520$ nm). Scale bar: 20 μm . The data are represented as mean \pm S.D. of three independent experiments. (* $p < 0.01$, compared with control).

showed a pronounced increase for the cells incubated with the CaO_2 nanoparticles (30 $\mu\text{g/mL}$), and the strongest fluorescence emission was observed for the cells treated with the $\text{CaO}_2@TA\text{-Fe}^{\text{III}}$ nanoconjugates (10 $\mu\text{g/mL}$). The above experimental results were also verified by flow cytometry experiments (Figures 4B–C). When 4T1 cells were incubated with the TA-Fe complex, the intracellular ROS level was very low and similar to that of the control group, while when the cells were incubated with CaO_2 nanospheres, the level of ROS in the cells was approximately 3 times higher than that of the control group, possibly due to the production of H_2O_2 by the decomposition of CaO_2 nanospheres. However, after the cells were treated with the $\text{CaO}_2@TA\text{-Fe}^{\text{III}}$ nanoconjugates, the intracellular ROS was approximately 20 times higher than that of the control group due to the enhanced Fenton reaction. Taken together, the above results indicated that the $\text{CaO}_2@TA\text{-Fe}^{\text{III}}$ nanoconjugates can produce a large amount of ROS in cells, and therefore have the potential for use in effective CDT on tumors.

Next, the generation of Ca^{II} in cells was detected using the Fluo-4 AM fluorescent probe. 4T1 cells were first incubated with the $\text{CaO}_2@TA\text{-Fe}^{\text{III}}$ nanoconjugates ($[\text{CaO}_2] = 10 \mu\text{g/mL}$) and CaO_2 nanospheres (10 $\mu\text{g/mL}$) for 4 h, respectively. Thereafter, the presence of Ca^{II} in cells was monitored by confocal laser scanning microscopy (CLSM) upon incubation with the Fluo-4 AM fluorescent probe. Figure 5 shows that only weak fluorescence emission of Fluo-4 AM was observed for the cells incubated with CaO_2 nanospheres, while the cells incubated with the $\text{CaO}_2@TA\text{-Fe}^{\text{III}}$ nanoconjugates showed strong fluorescence emission of Fluo-4 AM. These results also confirmed that the $\cdot\text{OH}$ produced by the Fenton reaction between Fe^{II} and H_2O_2 can induce oxidative stress for the cells, reducing the Ca^{II} carrying capacity of Ca^{II} protein, and leading to Ca^{II} enrichment in the cells and calcium overload.^[28]

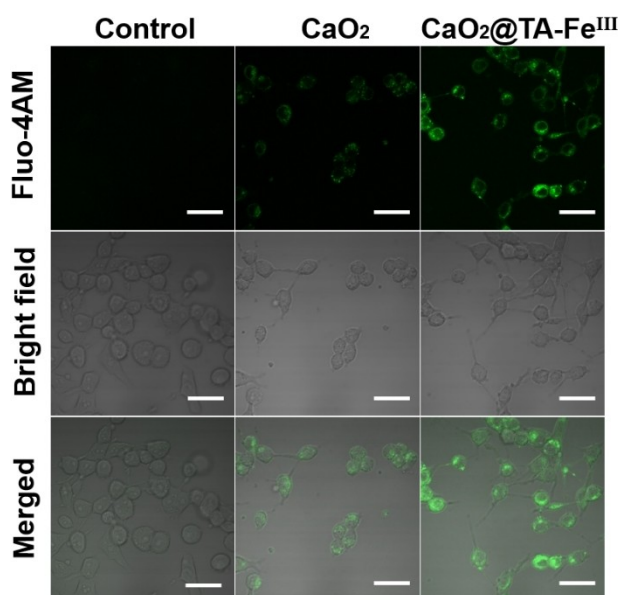


Figure 5. Fluorescence imaging of 4T1 cells treated with the CaO_2 nanoparticles or the $\text{CaO}_2@TA\text{-Fe}^{\text{III}}$ nanoconjugates, and the Fluo-4 AM fluorescent probe. Scale bar: 20 μm .

Evaluation of the cytotoxicity of $\text{CaO}_2@TA\text{-Fe}^{\text{III}}$ nanoconjugates

Next, the toxicity of the $\text{CaO}_2@TA\text{-Fe}^{\text{III}}$ nanoconjugates to the cells (4T1) was investigated by MTT experiments. As a control group, we also investigated the toxicity of the TA-Fe complex and the CaO_2 nanosphere agglomerates to 4T1 cells. As shown in Figure 6A, a cell survival rate of 83.8% was still obtained even for the 4T1 cells incubated with 30 $\mu\text{g/mL}$ of the TA-Fe complex for 24 h, suggesting that the TA-Fe complex has almost no toxicity to 4T1 cells at the concentration range of 0–30 $\mu\text{g/mL}$. Similarly, it is observed from Figure 6B that after incubating 4T1 cells with the CaO_2 nanosphere aggregates (30 $\mu\text{g/mL}$) for 24 h, a cell survival rate of 68.7% was still obtained, even though the CaO_2 nanoparticles decomposed to produce H_2O_2 . Interestingly, as shown in Figure 6C, a cell survival rate of only 11.2% was obtained for the 4T1 cells incubated with 10 $\mu\text{g/mL}$ of the $\text{CaO}_2@TA\text{-Fe}^{\text{III}}$ nanoconjugates for 24 h. These experimental results indicated that the

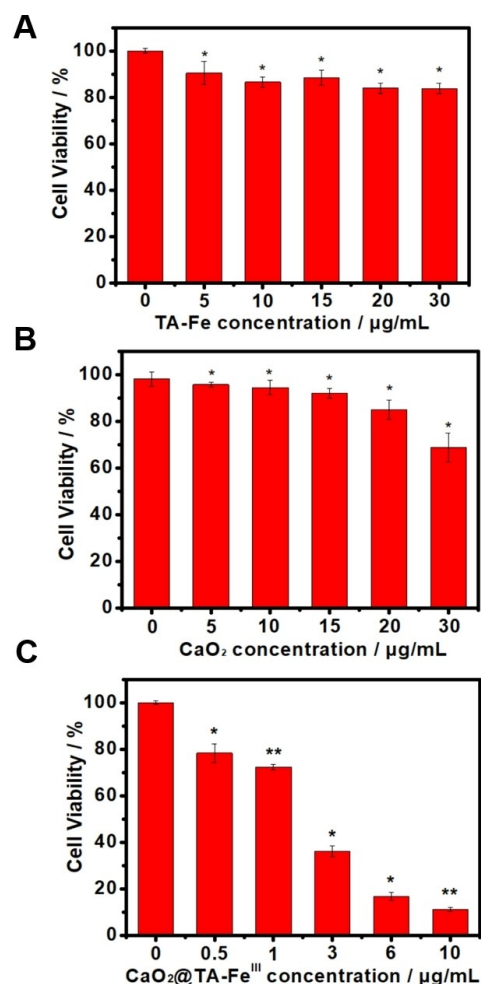


Figure 6. Viability of 4T1 cells after incubation with different concentrations of TA-Fe complex (A), CaO_2 nanosphere agglomerates (B), or $\text{CaO}_2@TA\text{-Fe}^{\text{III}}$ nanoconjugates (C) for 24 h. The data are represented as mean \pm S.D. of three independent experiments. (* $p < 0.05$, ** $p < 0.01$, compared with control).

CaO₂@TA-Fe^{III} nanoconjugates displays excellent cytotoxicity for tumor cells due to the synergistic effect of the TA-Fe complex system and the CaO₂ nanospheres.

Additionally, we also used fluorescent live/dead cell detection kit to further verify the cytotoxicity of the CaO₂@TA-Fe^{III} nanoconjugates. Figure 7 shows directly that after the 4T1 cell group was incubated with the CaO₂@TA-Fe^{III} nanoconjugates for 24 h, significant red fluorescence (representing dead cells) can be observed, while the other two 4T1 cell groups incubated with TA-Fe complex and the CaO₂ nanoparticles showed relatively pronounced green fluorescence (representing living

cells). The above experimental results were consistent with the results of the MTT experiments, and provided additional verification for the highly efficient cytotoxicity of the CaO₂@TA-Fe^{III} nanoconjugates on tumor cells.

Tumor therapy with the CaO₂@TA-Fe^{III} nanoconjugates

Finally, we investigated the anticancer effect of the CaO₂@TA-Fe^{III} nanoconjugates using the 4T1 tumor BALB/C mice as the model. During the treatment, the mice were weighed and the tumors' length and width were measured with an electronic ruler every two days. It is observed from Figures 8A–B that after 14 days of treatment, the tumors in the control group grew rapidly with the tumor volume reaching 7.9 times of the initial volume. Compared to the control group, the tumor volume grew more slowly for the groups treated with the TA-Fe complex and CaO₂ nanospheres, with the tumor volumes increasing by 6.6 times and 5.2 times after 14 days, respectively. By contrast, the group treated with the CaO₂@TA-Fe^{III} nanoconjugates showed little change and even a decrease in the tumor volume over 14 days, indicating the excellent tumor therapeutic efficacy of the CaO₂@TA-Fe^{III} nanoconjugates.

Moreover, there was no significant change in the body weight of the mice during treatment (Figure 8C), indicating that the CaO₂@TA-Fe^{III} nanoconjugates did not induce significant systemic toxicity. In addition, hematoxylin and eosin (H&E) staining (Figure 9) showed that the tumor tissue in the CaO₂@TA-Fe^{III} nanoconjugates-treated group was clearly damaged compared to the control group, providing further verification of the superior tumor treatment ability of the CaO₂@TA-Fe^{III} nanoconjugates. Meanwhile, no obvious morphological changes were observed in the main organs of all groups, including heart, liver, spleen, lung, and kidney, indicating that the CaO₂@TA-Fe^{III} nanoconjugates have the potential for development as a biocompatible therapeutic agent.

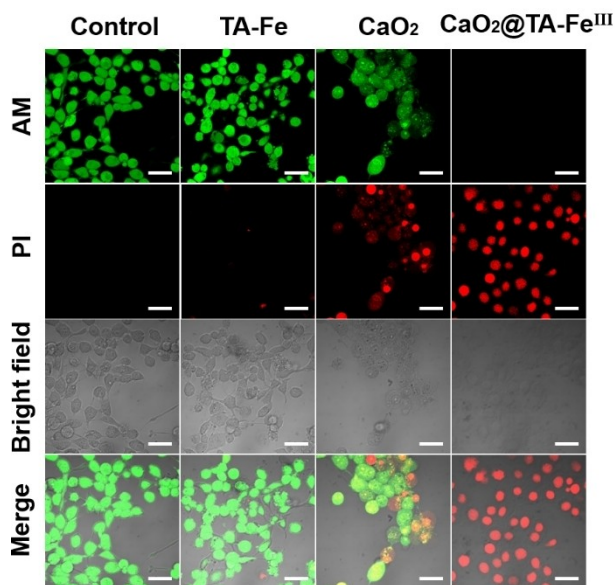


Figure 7. Fluorescence live/dead cell images of 4T1 cells incubated with the TA-Fe complex, CaO₂ nano spherical agglomerates, or the CaO₂@TA-Fe^{III} nanoconjugates for 24 h. Scale bar: 20 μm.

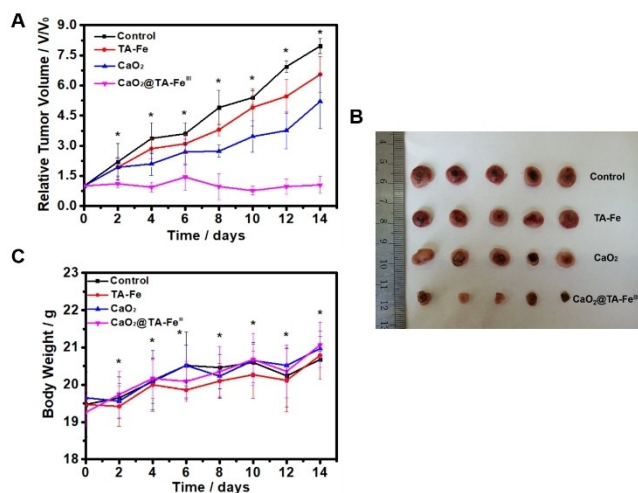


Figure 8. (A) Relative tumor volume changes and (B) Photographs of the tumors. (C) bodyweight changes for the mice groups received different treatments during the 14-days-treated process. The data are represented as mean ± S.D. of three independent experiments. (**p* < 0.01, compared with control).

Conclusion

In conclusion, we have prepared novel CaO₂@TA-Fe^{III} nanoconjugates which the generation of H₂O₂ depends on the lower

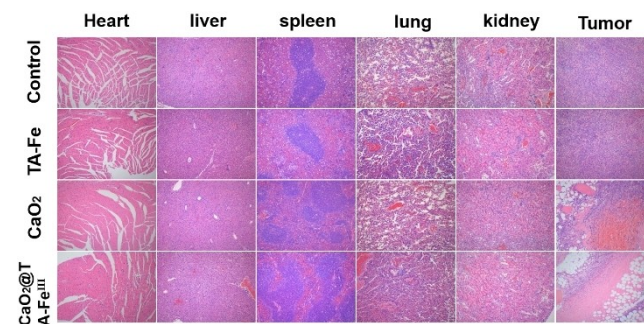


Figure 9. H&E staining of major organs and tumors for different mice groups after 14 days treatment.

pH conditions and TA can trigger the rapid conversion of Fe^{III} to Fe^{II}, thus greatly improving the efficiency of Fenton reaction under the acidic environment of the tumors. Meanwhile, the *OH produced during the Fenton reaction promote the calcium overload process, accelerating the apoptosis of cancer cells, and thus further enhancing the CDT effect of tumors. The results of *in vitro* and *in vivo* experiments showed that the CaO₂@TA-Fe^{III} nanoconjugates can effectively kill cancer cells and display an excellent tumor therapeutic effect. Therefore, we expect that the CaO₂@TA-Fe^{III} nanoconjugates can provide inspiration for the development of efficient anticancer reagents.

Experimental Section

Materials and instruments

Tannic acid (TA), ferric chloride hexahydrate (FeCl₃·6H₂O), polyvinylpyrrolidone (PVP, M.W. ≈ 58000), titanate sulphate (Ti (SO₄)₂) and ammonium hydroxide solution (25–28%) were purchased from Macklin Biochemical Co., Ltd. (China). Calcium chloride, 1,10-phenanthroline, methylene blue (MB), hydrogen peroxide (H₂O₂, 30%) were obtained from Sinopharm Group Chemical Reagent Co., Ltd. (China). 2',7'-dichlorofluorescein diacetate (DCFH-DA) and Fluo-4 AM were purchased from Beyotime Biotechnology (China).

Transmission electron microscopy (TEM) images were obtained using a JEOL-3010 microscope. The zeta potential and hydrodynamic size analysis was performed using a Zetasizer (Nano-Z, Malvern, UK). The XRD analysis was performed with a powder X-ray diffractometer (D8Advance, Bruker, Germany) using Cu K α radiation. Fourier transform infrared (FT-IR) spectra were collected with a Fourier transform infrared spectrometer (SENSOR27, Germany). Confocal microscopy images were obtained using an Olympus FV1000-MPE multiphoton laser scanning confocal microscope (Olympus, Japan). Flow cytometry analysis was carried out using a FACScan cytometer (Becton Dickinson Immunocytometry Systems, San Jose, CA). UV-vis absorption spectra were acquired using a UV-vis spectrophotometer (U-4100, Japan).

Synthesis of CaO₂ nanosphere agglomerates

CaO₂ nanosphere agglomerates were synthesized according to the synthetic method reported in a previous study.^[43] Briefly, the steps of this method are as follows: first, anhydrous calcium chloride (100 mg) and polyvinylpyrrolidone (350 mg) are weighed and dissolved in absolute ethanol (10 mL), sonicated and dissolved. After stirring at room temperature for 30 min, ammonia water (0.8 M, 1 mL) is added and the solution is stirred for 5 min, and then H₂O₂ (200 μ L, 1 M) is slowly added, and the stirring is continued for 20 min. At this time, the solution changed from colourless to light blue, indicating that CaO₂ nanospheres were obtained. The light blue solution was collected, centrifuged at 15,000 rpm for 15 min, and washed three times with ethanol.

Synthesis of CaO₂@TA-Fe^{III} nanoconjugates

CaO₂ nanosphere agglomerates (3.5 mg) were dissolved in absolute ethanol (5 mL), and a FeCl₃ solution (1 mL, 1.3 mg/mL) was added to the CaO₂ solution, and sonicated for 10 seconds, followed by the addition of the TA solution (1 mL, 2.5 mg/mL) and sonication for 10 seconds. The color of solution turned brown-black. The product was collected by centrifugation at 13000 rpm for 10 min, and was

washed three times with absolute ethanol to obtain the CaO₂@TA-Fe^{III} nanoconjugates.

Decomposition of CaO₂ nanoparticles under various pH conditions

The content of H₂O₂ produced by the decomposition of CaO₂ in buffer with different pH was determined by the titanium sulphate colorimetric method.^[45] First, solutions (300 μ L) with different concentrations of H₂O₂ were mixed evenly with a titanium sulphate solution (1%, 300 μ L). After 10 min, the absorption of the mixture solution was measured at 410 nm with an ultraviolet instrument to obtain a standard curve. Then, the dialysis bags containing CaO₂ nanoparticles were placed into PBS buffer (20 mL) with different pH (pH 7.4, 6.0, 5.0) and were shaken steadily at 37 °C. At different times between 0 and 48 h, a volume of the buffer solution (300 μ L) was removed, and fresh buffer (300 μ L) was added to replace the removed buffer. Then, according to the standard curve, the percentage of H₂O₂ produced by the decomposition of CaO₂ in buffer solutions at different pH was calculated.

Verification of Fe^{II} generation by the CaO₂@TA-Fe^{III} nanoconjugates

The release of Fe^{II} at different times was measured by 1,10-phenanthroline colorimetry.^[40] First, FeCl₃ solutions (200 μ L) with different concentrations were mixed with ascorbate acid (10 mM, 200 μ L), and incubated at room temperature for 3 min, and then 1,10-phenanthroline (200 μ L, 1 mg/mL) was added, and the absorption of the mixture solution at 510 nm was detected using a UV-vis spectrometer after 10 min. Finally, the standard curve was obtained.

Next, the samples (1 mL) were placed in dialysis bags, and the dialysis bags were immersed in buffer solutions (20 mL) with different pH (pH 7.4, 6.0, 5.0). At different times (30, 60, 120, and 180 min), a sample of the dialysis buffer (200 μ L) was removed and fresh buffer (200 μ L) was added. After reacting with 1,10-phenanthroline for 10 min, the absorption of the mixture solution at 510 nm was measured with a UV-vis spectrometer.

Investigation of Fenton reaction with CaO₂@TA-Fe^{III} nanoconjugates *in vitro*

First, MB solution (60 μ L) and H₂O₂ solution (40 μ L, for the control group, 40 μ L of ultrapure water was used) were added into the CaO₂@TA-Fe^{III} nanoconjugates (or TA-Fe complex)-containing phosphate buffer solutions (300 μ L) with different pH (pH 7.4, 6.0, 5.0). In this mixture solution, the final concentrations of the CaO₂@TA-Fe^{III} nanoconjugates (or TA-Fe complex), H₂O₂ and MB were 100 μ g/mL, 200 μ M, and 30 μ g/mL, respectively. Then, the absorbance of MB at 664 nm was measured at different times (30, 60, 90, 120, 150, and 180 min).

Cell uptake of the CaO₂@TA-Fe^{III} nanoconjugates

First, 4T1 cells were cultured in a cell incubator containing Dulbecco's modified Eagle's medium (DMEM) with 10% foetal bovine serum (FBS) and 1% antibiotics (penicillin/streptomycin) under 5% CO₂, 37 °C. Then, the 4T1 cells were planted in the confocal culture dish and incubated for 24 h. After that, the culture medium was replaced by fresh culture medium containing FITC labelled CaO₂@TA-Fe^{III} nanoconjugates (10 μ g/mL) and further incubated for 2, 4, and 8 h, respectively. Then, the green

fluorescence emission of the cells was monitored with a confocal laser scanning microscope (CLSM).

MTT assay

The 4T1 cells were seeded in 96-well plates. After incubation for 24 h, the culture medium in the 96-well plates was aspirated, and then fresh culture medium (200 μ L) containing different concentrations of TA-Fe complex, CaO₂ nanospheres (ranging from 5 to 30 μ g/mL), and CaO₂@TA-Fe^{III} nanoconjugates (ranging from 0.5 to 10 μ g/mL) was added to each well. After incubation for 24 h, the culture medium was precipitated and washed with sterile PBS, and then an MTT solution (60 μ L, 0.5 mg/mL) was added into each well. After incubation for 4 h, the MTT solution was aspirated slowly, then DMSO (100 μ L) was added to each well, and finally the absorbance of the solution at 490 nm was measured with a microplate reader.

Evaluation of live/dead cells through AM/PI experiments

The 4T1 cells were seeded in the confocal culture dish and incubated at 37 °C for 24 h. The culture medium was replaced by fresh culture medium containing TA-Fe^{III} complex (30 μ g/mL), CaO₂ nanospheres (30 μ g/mL), and CaO₂@TA-Fe^{III} nanoconjugates (10 μ g/mL), respectively. The cells were incubated for another 24 h, and then, the cell culture solution was removed and a fresh culture solution containing AM/PI double stain was added. After incubation for 30 min, the sample was washed twice with PBS. Finally, intracellular fluorescence was monitored by CLSM.

Measurement of intracellular ROS with CLSM and flow cytometry

The 4T1 cells were planted in a 6-well plate and incubated for 24 h. The culture medium was replaced by fresh culture medium containing TA-Fe complex, CaO₂ nanospheres, CaO₂@TA-Fe^{III} nanoconjugates, respectively. After incubation for 4 h, the culture medium was sucked out and washed with PBS. Then, fresh culture medium (1 mL) containing DCFH-DA (10 μ g/mL) was added to each well, and after incubation for 30 min, the culture medium was sucked out and washed with PBS. Finally, the fluorescence emission of the cells was measured using CLSM. Meanwhile, the cells were collected and dispersed in PBS (500 mL) for flow cytometry.

Measurement of intracellular Ca^{II}

4T1 cells were first seeded in the confocal culture dish and incubated at 37 °C for 24 h. Then, the culture medium was replaced by fresh culture medium containing CaO₂ nanospheres (10 μ g/mL), or CaO₂@TA-Fe^{III} nanoconjugates ([CaO₂] = 10 μ g/mL), and incubated for another 4 h. Then, the cell culture solution was removed and fresh culture solution containing Fluo-4 AM fluorescence probe (4 μ M) was added. After incubation for 30 min, the sample was washed with PBS. Finally, fluorescence emission of the cells was monitored by CLSM.

Tumor therapy with the CaO₂@TA-Fe^{III} nanoconjugates

The 4T1 tumor BALB/female mice were randomly divided into 4 groups (5 mice in each group). When the tumor volume grew to about 100 mm³, the 4 groups were intermittently injected every other day (for a total of three times) with different materials (PBS, TA-Fe complex, CaO₂ nanospheres, CaO₂@TA-Fe^{III} nanoconjugates at an equal dose of 7.5 mg/kg). Subsequently, the weight of the

mouse and the length and width of the tumor were measured every two days. The tumor volume was calculated according to the formula $V = L \times W^2 / 2$. After 14 days of treatment, mice tumors and major organs (heart, liver, spleen, lung, kidney) were collected for further analysis.

Acknowledgements

This work was supported by NSFC (21775035), Hunan Provincial Science and Technology Foundation(2020SK2096), and Changsha Municipal Natural Science Foundation (Kq2014149).

Conflict of Interest

The authors declare no conflict of interest.

Keywords: Chemodynamic therapy · Calcium peroxide · Tannic acid · Fenton reaction · Calcium overload

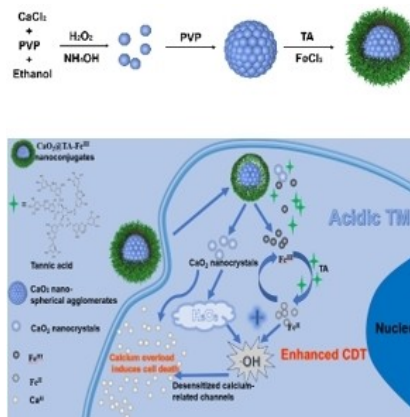
- [1] K. H. Thompson, C. Orvig, *Science* **2003**, *300*, 936–939.
- [2] I. Ivanovic-Burmazovic, *Inorg. React. Mech.* **2013**, *1*, 1–2.
- [3] E. D. Weinberg, *Eur. J. Cancer Prev.* **1996**, *5*, 19–36.
- [4] P. T. Lie, M. Heiskala, P. A. Peterson, *Mol. Aspects Med.* **2001**, *22*, 1–87.
- [5] S. Okada, *Pathol. Int.* **1996**, *46*, 311–33.
- [6] J. Prousek, *Pure Appl. Chem.* **2007**, *79*, 2325–2338.
- [7] A. Bokare, W. Choi, *J. Hazard. Mater.* **2014**, *275*, 121–135.
- [8] A. L. Fracanzani, D. Conte, M. Fraquelli, *Hepatology.* **2001**, *33*, 647–651.
- [9] X. Qian, J. Zhang, Z. Gu, Y. Chen, *Biomaterials.* **2019**, *211*, 1–13.
- [10] Y. X. Guo, X. D. Zhang, W. Sun, H. R. Jia, Y. X. Zhu, X. P. Zhang, N. X. Zhou, F. G. Wu, *Chem. Mater.* **2019**, *31*, 10071–10084.
- [11] G. Shen, R. Xing, N. Zhang, *ACS Nano* **2016**, *10*, 5720–5729.
- [12] D. W. Zheng, Q. Lei, J. Y. Zhu, *Nano Lett.* **2016**, *17*, 284–291.
- [13] M. Valko, C. J. Rhodes, J. Moncol, *Chem.-Biol. Interact.* **2006**, *160*, 1–40.
- [14] M. Munoz, Z. M. D. Pedro, J. A. Casas, *Appl. Catal. B* **2015**, *176*, 249–265.
- [15] E. Novo, M. Parola, *Fibro. Tissure. R.* **2008**, *1*, 5.
- [16] P. Chiarugi, P. Cirri, *Trends Biochem. Sci.* **2003**, *28*, 509–514.
- [17] T. Finkel, *J. Cell Biol.* **2011**, *194*, 7–15.
- [18] J. Cadet, T. Douki, J. L. Ravanat, *Free Radical Biol. Med.* **2010**, *49*, 9–21.
- [19] J. Kim, H. R. Cho, H. Jeon, D. Kim, C. Y. Song, N. Lee, S. H. Choi, T. Hyeon, *J. Am. Chem. Soc.* **2017**, *139*, 10992–10995.
- [20] L. F. Tan, J. Wan, W. S. Guo, C. Z. Ou, T. L. Liu, C. H. Fu, Q. Zhang, X. L. Ren, X. J. Liang, J. Ren, L. F. Li, X. W. Meng, *Biomaterials.* **2018**, *159*, 108–118.
- [21] Q. Wang, S. Tian, N. Ning, *Ind. Eng. Chem. Res.* **2013**, *53*, 643–649.
- [22] W. Shi, D. Du, B. Shen, C. F. Cui, L. J. Lu, L. Z. Wang, J. L. Zhang, *ACS Appl. Mater. Interfaces* **2016**, *8*, 20831–20838.
- [23] L. S. Lin, J. B. Song, L. Song, K. M. Ke, Y. J. Liu, Z. J. Zhou, Z. Y. Shen, J. Li, Z. Yang, W. Tang, G. Niu, H. H. Yang, X. Y. Chen, *Angew. Chem. Int. Ed.* **2018**, *57*, 4902–4906; *Angew. Chem.* **2018**, *130*, 4996–5000.
- [24] L. Wang, M. Huo, Y. Chen, J. Shi, *Biomaterials.* **2018**, *163*, 1–13.
- [25] L. S. Lin, T. Huang, J. B. Song, X. Y. Ou, Z. T. Wang, H. Z. Deng, R. Tian, Y. J. Liu, J. F. Wang, Y. Liu, G. C. Yu, Z. J. Zhou, S. Wang, G. Niu, H. H. Yang, X. Y. Chen, *J. Am. Chem. Soc.* **2019**, *141*, 9937–9945.
- [26] C. H. Liu, D. D. Wang, S. Y. Zhang, Y. R. Cheng, F. Yang, Y. Xing, T. L. Xu, H. F. Dong, X. J. Zhang, *ACS Nano* **2019**, *13*, 4267–4277.
- [27] A. Xu, X. Li, S. Ye, G. Yin, Q. Zeng, *Appl. Catal. B* **2011**, *102*, 37–43.
- [28] M. Zhang, R. X. Song, Y. Y. Liu, Z. G. Yi, X. F. Meng, J. W. Zhang, Z. M. Tang, Z. W. Yao, Y. Liu, X. G. Liu, W. B. Bu, *Chem.* **2019**, *5*, 2171–2182.
- [29] S. Hong, J. Yeom, I. T. Song, S. M. Kang, H. Lee, H. Lee, *Adv. Mater. Interfaces.* **2014**, *1*, 1400113.
- [30] J. H. Waite, M. L. Tanzer, *Science.* **1981**, *212*, 1038–1040.
- [31] J. Li, S. X. Wu, C. C. Wu, L. P. Qiu, G. Z. Zhu, C. Cui, Y. Liu, W. J. Hou, Y. Y. Wang, L. Q. Zhang, L. Teng, H. H. Yang, W. H. Tan, *Nanoscale.* **2016**, *8*, 8600–8606.

- [32] T. S. Sileika, D. G. Barrett, R. Zhang, K. Hang, A. Lau, P. B. Messersmith, *Angew. Chem. Int. Ed.* **2013**, *52*, 1076–10770; *Angew. Chem.* **2013**, *125*, 10966–10970.
- [33] S. A. Abouelmagd, F. F. Meng, B. K. Kim, H. Hyun, Y. Yeo, *ACS Biomater. Sci. Eng.* **2016**, *2*, 2294–2303.
- [34] J. L. Guo, Y. Ping, H. Ejima, K. Alt, M. Meissner, J. J. Richardson, Y. Yan, K. Peter, D. V. Elverfeldt, A. Christoph, H. F. Caruso, *Angew. Chem. Int. Ed.* **2014**, *53*, 5546–5551; *Angew. Chem.* **2014**, *126*, 5652–5657.
- [35] H. Ejima, J. J. Richardson, K. Liang, J. P. Best, M. P. van Koeverden, G. K. Such, J. Cui, F. Caruso, *Science* **2013**, *341*, 154–157.
- [36] H. A. Huang, P. Li, C. L. Liu, H. L. Ma, H. Huang, Y. C. Lin, C. Wang, Y. L. Yang, *RSC Adv.* **2017**, *7*, 2829–2835.
- [37] S. Kim, S. Philippot, S. Fontanay, R. E. Duval, E. Lamouroux, N. Canilho, A. Pasc, *RSC Adv.* **2015**, *5*, 90550–90558.
- [38] H. S. Liang, J. Li, Y. He, W. Xu, S. L. Liu, Y. Li, Y. J. Chen, B. Li, *ACS Biomater. Sci. Eng.* **2016**, *2*, 317–325.
- [39] Y. Ping, J. Guo, H. Ejima, *Small* **2015**, *11*, 2032–2036.
- [40] L. Zhang, S. S. Wan, C. X. Li, L. Xu, H. Cheng, X. Z. Zhang, *Nano Lett.* **2018**, *18*, 7609–7618.
- [41] P. Pinton, C. Giorgi, R. Siviero, E. Zecchini, R. Rizzuto, *Oncogene*. **2008**, *27*, 6407–6418.
- [42] G. Ermak, K. J. Davies, *Mol. Immunol.* **2002**, *38*, 713–721.
- [43] S. Shen, M. Mamat, S. C. Zhang, J. Cao, Z. D. Hood, L. Figueroa-Cosme, Y. N. Xia, *Small* **2019**, *15*, 1902118.
- [44] S. S. Madan, K. L. Wasewar, C. R. Kumar, *Adv. Powder Technol.* **2016**, *27*, 2112–2120.
- [45] J. Kim, H. R. Cho, H. Jeon, D. Kim, C. Song, N. Lee, S. H. Choi, T. Hyeon, *J. Am. Chem. Soc.* **2017**, *139*, 10992.
- [46] A. Northup, D. P. Cassidy, *J. Hazard. Mater.* **2008**, *152*, 1164–1170.
- [47] Y. Guo, H. R. Jia, X. Zhang, *Small*. **2020**, *1*, 2000897.

Manuscript received: February 10, 2021
Accepted manuscript online: April 1, 2021
Version of record online: ■■■, ■■■■

FULL PAPERS

To solve the problem of low efficiency of Fenton reaction catalyst and insufficient endogenous H_2O_2 content in chemodynamic therapy, we designed a Fenton nanosystem with excellent catalytic performance that can provide H_2O_2 by itself. The tannic acid (TA)-Fe nanocoating formed by TA and Fe^{III} was combined with CaO_2 to construct a $\text{CaO}_2@TA\text{-Fe}^{\text{III}}$ nanosystem with pH-response characteristics. At the same time, the occurrence of the "calcium overload" process can further enhance the antitumor therapeutic effect.



F. Chen, B. Yang, L. Xu, Prof. J. Yang*, Prof. J. Li*

1 – 10

A $\text{CaO}_2@Tannic\ Acid\text{-Fe}^{\text{III}}$ Nanoconjugate for Enhanced Chemodynamic Tumor Therapy

